AIP | Journal of Applied Physics

Electron transport and band structure in phosphorus-doped polycrystalline silicon films

David L. Young, Howard M. Branz, Fude Liu, Robert Reedy, Bobby To et al.

Citation: J. Appl. Phys. **105**, 033715 (2009); doi: 10.1063/1.3068349
View online: http://dx.doi.org/10.1063/1.3068349
View Table of Contents: http://jap.aip.org/resource/1/JAPIAU/v105/i3
Published by the American Institute of Physics.

Related Articles

Effect of indirect interband absorption in Ge/SiGe quantum wells
J. Appl. Phys. 110, 083119 (2011)

Optical gain in short period Si/Ge superlattices on [001]-SiGe substrates
J. Appl. Phys. 110, 083105 (2011)

Investigation of thermal transport degradation in rough Si nanowires
J. Appl. Phys. 110, 074510 (2011)

Diffusion of E centers in germanium predicted using GGA+U approach
Appl. Phys. Lett. 99, 072112 (2011)

Effective masses and electronic structure of diamond including electron correlation effects in first principles calculations using the GW-approximation
AIP Advances 1, 032139 (2011)

Additional information on J. Appl. Phys.

Journal Homepage: http://jap.aip.org/
Journal Information: http://jap.aip.org/about/about_the_journal
Top downloads: http://jap.aip.org/features/most_downloaded
Information for Authors: http://jap.aip.org/authors

ADVERTISEMENT

AIPAdvances
Submit Now
Explore AIP's new open-access journal
• Article-level metrics now available
• Join the conversation! Rate & comment on articles

Downloaded 21 Nov 2011 to 147.8.21.59. Redistribution subject to AIP license or copyright; see http://jap.aip.org/about/rights_and_permissions

JOURNAL OF APPLIED PHYSICS **105**, 033715 (2009)

Electron transport and band structure in phosphorus-doped polycrystalline silicon films

David L. Young,[a] Howard M. Branz, Fude Liu, Robert Reedy, Bobby To, and Qi Wang
National Renewable Energy Laboratory, 1617 Cole Boulevard, Golden, Colorado 80401, USA

(Received 25 July 2008; accepted 8 December 2008; published online 10 February 2009)

We study transport mechanisms, effective mass, and band structure by measuring the resistivity, Hall, and Seebeck and Nernst coefficients in heavily phosphorus-doped polycrystalline silicon films made by thermal crystallization of amorphous silicon. We observe a change in transport mechanism which results in an increase in electron mobility from 10% to 80% of the single-crystal silicon mobility as the carrier concentration increases from 10^{19} to 10^{20} cm^{-3}. Our measurements of effective mass at the Fermi level indicate that as the carrier concentration increases, there is a shift from impurity-band transport to conduction-band transport, and that the electron effective mass is lower in the impurity band than in the conduction band of Si. The shift to conduction-band transport improves electron mobility with carrier density by improving intragrain carrier mean free path lengths and relaxation times. © *2009 American Institute of Physics*. [DOI: 10.1063/1.3068349]

I. INTRODUCTION

Mott[1] proposed that impurity bands will form when the density of impurities with electronic levels within an insulator bandgap exceeds a minimum concentration (about 10^{17} cm^{-3} in silicon[2]). At this "Mott transition," wave function overlap creates extended states and the zero-temperature mobility becomes finite. The Mott transition is observed in many systems.[3] Recent measurements of the temperature dependence of magnetic susceptibility on *n*-type silicon[4–6] have suggested that further increases in impurity density can broaden the impurity band until it overlaps with the conduction band. At this density, one would expect dramatic changes in transport properties.[2] In this paper, we present a direct measurement of this change in transport, through a study of resisitivity and the Hall, Seebeck, and Nernst coefficients in *n*-type polycrystalline Si. Our measurements probe the mobility and, for the first time, effective mass within the *P*-impurity band in silicon which give insights into the transport mechanisms in polycrystalline Si (poly-Si).

Solid-phase crystallization (SPC) of hydrogenated amorphous silicon (*a*-Si:H) films on low-temperature substrates enhances the mobility and eliminates light-induced degradation that limits the utility of *a*-Si:H in some applications. As a result, poly-Si films are now being used industrially for high-speed transistors[7] and efficient, low-cost solar cells.[8,9] Poly-Si films can be highly doped to serve as transparent contacts in a device—replacing the transparent conducting oxide (TCO) layers usually used in thin-film photovoltaics. The electron transport performance of highly doped poly-Si films is similar to TCOs, with mobilities above 50 $cm^2/V\,s$, carrier concentrations (ccs) in the low 10^{20} cm^{-3}, and resistivities of 10^{-4} Ω cm. The added benefit of forming a chemically stable, all-Si-based thin-film solar cell[10] may outweigh the slightly poorer transport properties and optical transparency of the poly-Si materials compared to TCOs.

We have measured the structure and electronic properties in heavily phosphorus-doped poly-Si films. These films are formed by hot-wire chemical vapor deposition (HWCVD) of *a*-Si:H(P), followed by a thermal SPC. Structure-related measurements include x-ray diffraction (XRD), and electron back scatter diffraction. Transport measurements include Seebeck and Nernst coefficients and the temperature-dependent measurements of resisitivity and Hall coefficients. The method of four coefficients[11] (MFC) then permits us to calculate the carrier density, mobility, mean free path, relaxation time, and effective mass.

II. FILM GROWTH, CRYSTALLIZATION, AND STRUCTURE

The *n*-type, phosphorus-doped *a*-Si:H films were grown by the HWCVD process using a 0.051 cm diameter tungsten filament heated with 16 A (about 2000 °C) to decompose a mixture of SiH_4 and 5% PH_3 in H_2 gas onto a heated substrate 5 cm from the filament. Deposition pressure was held at 10 mT with flow rates of 20 SCCM (SCCM denotes cubic centimeter per minute at STP) for SiH_4 and 3 SCCM for 5% PH_3 in H_2. 1 $in.^2$ 1737 Corning glass was used as a substrate and heated, before growth began, to nominal deposition temperatures (T_d) between 150 and 800 °C, using an infrared heating element. T_d was measured by a thermocouple pressed to the deposition surface of the substrate. Measured and actual temperatures of the deposited films may differ significantly due to the experimental difficulty of accurately measuring thin-film temperatures in a vacuum due to significant radiative heating from the hot filament. No barrier layers were used between the glass substrate and the *a*-Si:H film. Growth rates were between 10 and 27 Å/s with most films grown to a thickness of about 1 μm. Two sets of *a*-Si:H films were grown in the same reactor at nearly identical growth conditions and then annealed until fully crystallized. One set was annealed at 580 °C and the other set was annealed at 600 °C (details below).

[a]Electronic mail: david_young@nrel.gov.

 © 2009 American Institute of Physics

Downloaded 21 Nov 2011 to 147.8.21.59. Redistribution subject to AIP license or copyright; see http://jap.aip.org/about/rights_and_permissions

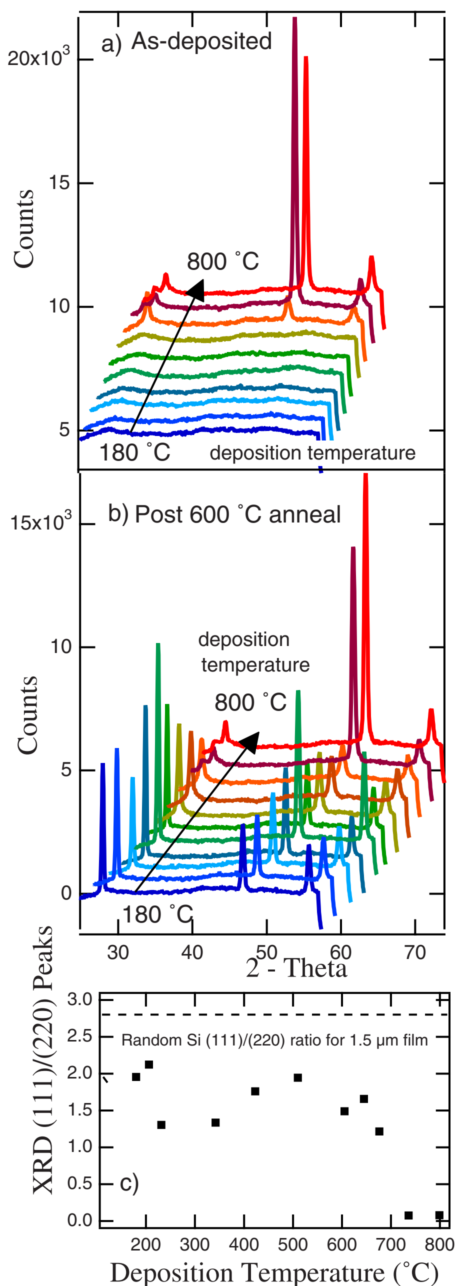

FIG. 1. (Color online) XRD results for (a) as-deposited films and (b) films annealed at 600 °C. Graph (c) shows the (111)/(220) XRD peak ratio for crystallized films as a function of deposition temperature, with the expected ratio for randomly oriented crystallites in a 1.5 μm thick c-Si film indicated by the horizontal dashed line (Ref. 29). Strong (220) orientation occurs for films grown above 675 °C.

XRD patterns were measured on a Bruker D8 Discover instrument and are shown in Fig. 1. As-deposited films grown below 675 °C were amorphous by XRD. However, films grown above 675 °C were single-phase polycrystalline silicon with a strong (220) orientation, even before annealing [Fig. 1(a)].

Elemental depth profiles of C, H, O, and P were measured by secondary ion mass spectrometry on both sets of as-deposited films. Concentrations of unintentional C, H, and O varied widely in the films as a function of deposition temperature and between nominally identical depositions, with C concentrations typically lower than H or O concentrations. However, no correlation between H, O, or C impurity concentrations and grain size or postannealing electronic properties was seen. The C, H, and O impurities in the films were generally more uniformly distributed through the films annealed at 580 °C than through the films annealed at 600 °C. The extrinsic n-type dopant, phosphorus, was incorporated quite uniformly throughout the bulk of each film. P concentrations were nearly constant at 8×10^{20} cm^{-3} in the films annealed at 580 °C, but varied between 2 and 4 $\times10^{20}$ cm^{-3} in the films annealed at 600 °C. We have observed that P-content does not change during crystallization of a-Si:H films; thus, the present variations in P concentration most likely arose during growth rather than during annealing.

As-deposited films were annealed at either 580 or 600 °C in a N_2 environment in a tube furnace, until fully crystallized. *In situ* optical reflectivity with automated computer analysis[12] was used to monitor the state of crystallization during the annealing. Previous work showed that films have H concentrations [H] well below 0.1 at. % after annealing.[13]

XRD results in Figs. 1(b) and 1(c) show that postannealed samples appear fully crystallized with only a slight (220) orientation at $T_d<675$ °C. There is a strong (220) orientation for deposition temperatures greater than 675 °C. Further postdeposition annealing of these high-temperature samples did not change the peak intensities or (111)/(220) peak ratios, significantly. All films crystallized during annealing.

Electron backscatter diffraction (EBSD) images reveal the grain size and grain orientation of the top surface of some of our films. A typical EBSD image is shown in Fig. 2(a), from a film deposited at 510 °C. EBSD shows large (>1 μm), randomly oriented grains imbedded in a matrix of much smaller grains. Figure 2(b) shows the same image as in Fig. 2(a) with grains smaller than 0.8 μm diameter removed. This image clearly shows that some of the large grains are isolated from other large grains by micron-scale boundary regions dominated by small grains. The EBSD images were analyzed by modeling software to determine the size distribution of all grains over 0.8 μm diameter and these results are shown in Fig. 2(c). The average grain size decreases with T_d. The largest grains imaged in a 10×15 μm^2 area are between 3 and 6.5 μm in linear dimension. However, as the films begin to exhibit strong (220) orientation at $T_d>675$ °C, the surface roughness of the films becomes too large for grain size measurements by EBSD. For example, a film grown at 605 °C has a surface roughness, measured by atomic force microscopy (AFM), of only 0.94 nm, but a film grown at 736 °C has an AFM roughness of 24 nm due to sharp, needlelike crystalline formations on the surface of the film. Scherrer formula analysis[14] of the full width at half maximum XRD (220) peak showed no systematic boardening as a function of deposition temperature for all of our samples (peak boardening for $T_d\sim200$ °C is similar to $T_d\sim800$ °C). We conclude that all samples have similar order-of-magnitude grain sizes consistent with Fig. 2(c).

Downloaded 21 Nov 2011 to 147.8.21.59. Redistribution subject to AIP license or copyright; see http://jap.aip.org/about/rights_and_permissions

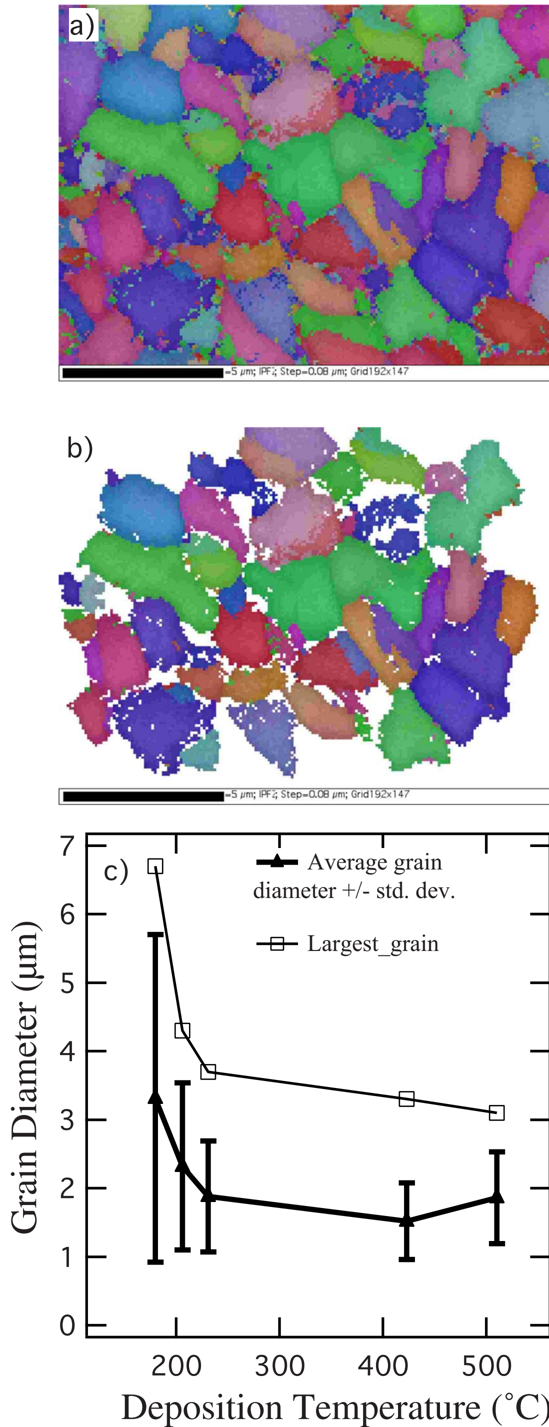

FIG. 2. (Color online) (a) EBSD image of film grown at 510 °C and crystallized at 600 °C, red=⟨100⟩, green=⟨110⟩, blue=⟨111⟩, with other orientations also shown by colors. (b) Same image as (a) with grains smaller than 0.8 μm removed. (c) Average grain size and largest imaged grain as a function of deposition temperature.

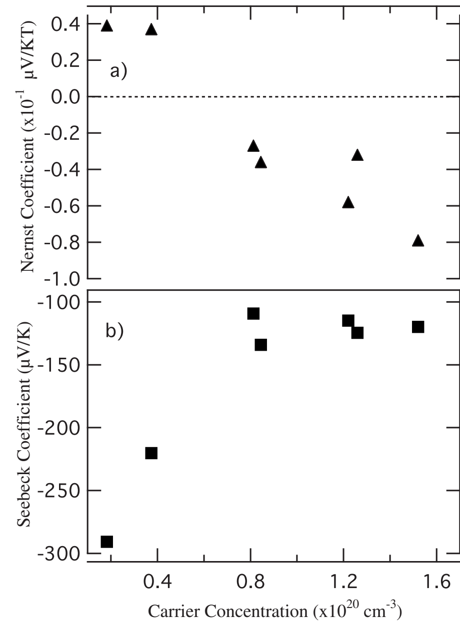

FIG. 3. (a) Nernst and (b) Seebeck coefficients as a function of cc.

III. ELECTRON TRANSPORT BY THE MFC

Electron transport studies were performed on the crystallized films using the MFC, where the resistivity and the Hall, Seebeck, and Nernst coefficients are measured on the same sample.[11] In TCO materials, with n and μ similar to our poly-Si films, the MFC technique was found to be ideal for revealing the dominant scattering mechanism and the density-of-state (DOS) effective mass at the Fermi level.[15]

The as-deposited films grown at $T_d < 736$ °C could not be studied by MFC due to their low mobilities and high resistivities before crystallization. However, the as-deposited films grown above 736 °C had Hall effect cc, resistivity, and mobility comparable to the crystallized lower-T_d films. Crystallized films grown at $T_d > 200$ °C were easily measured by MFC presumably due to the existence of large c-Si grains [Fig. 2(a)]. Films grown at $T_d < 200$ °C cracked during annealing, probably due to rapid H effusion; these could not be measured by MFC. We did not employ H-passivation or defect annealing by rapid thermal processing, although each can improve carrier transport properties in some poly-Si films.[16]

Figures 3(a) and 3(b) show the variation in the Nernst and Seebeck coefficients with carrier density. The Seebeck values, and their increase with decreasing carrier density, are typical for n-type semiconducting materials. The Nernst coefficient undergoes a sign change for the lowest carrier density films ($T_d > 730$ °C) indicating a possible change in scattering mechanism.[17] Figure 4(a) shows the effect of T_d on the cc, n, determined by Hall measurement. The carrier density peaks at $\sim 1.5 \times 10^{20}$ cm^{-3} at 400 °C and gradually decreases to $\sim 10^{19}$ cm^{-3} for deposition temperatures near 800 °C. The fraction of active dopants varied between 20% and 38% for films deposited below ~600 °C, but is less than 12% for films grown at $T_d > 600$ °C. These dopant activation fractions are low compared to laser-crystallized films (nearly 100% doping efficiency);[4] we attribute this to our much lower annealing temperatures. Figure 4(b) shows the effect of deposition temperature on electron mobility. Both cc [Fig. 4(a)] and mobility are highest at ~400 °C in our sample set. Figure 4(c) displays the mean free path length l of free carriers as a function of deposition temperature calculated from $l = \mu\hbar / q(3\pi^2 n)^{1/3}$. Figure 4(d) shows how the relaxation time [time between scattering events, as calculated from ($\tau = \mu m^*/q$)] changes with deposition temperature, where μ is the mobility (Hall effect), q is the electron charge, and m^* is

Downloaded 21 Nov 2011 to 147.8.21.59. Redistribution subject to AIP license or copyright; see http://jap.aip.org/about/rights_and_permissions

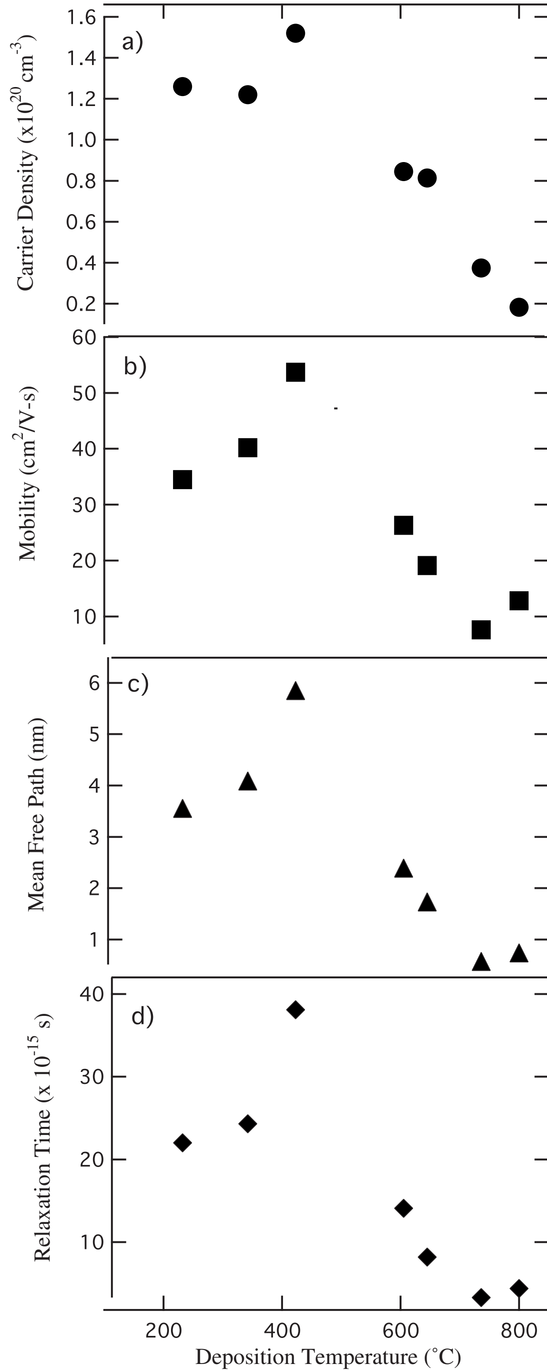

FIG. 4. (a) Carrier density, (b) mobility, (c) mean free path, and (d) relaxation time as a function of deposition temperature, after crystallization at 600 °C.

the electron effective mass (by MFC). Both relaxation time and mean free path are largest at $T_d \sim 400$ °C. In Fig. 5, we replot the mobility against cc and see a linear increase in μ with n. The dotted curve in Fig. 5 shows the literature values[18] for μ versus n in P-doped single-crystal Si (c-Si:P). Remarkably, the mobility values in our poly-Si films approach 82% those of c-Si:P at higher ccs.

Figure 6 shows mobility versus measurement temperature T of samples grown at different T_d. Selected curves are labeled by their room-temperature ccs; the highest n samples generally have higher μ (see also Fig. 5). The mobility increases slightly with T at the low ccs, but as carrier density

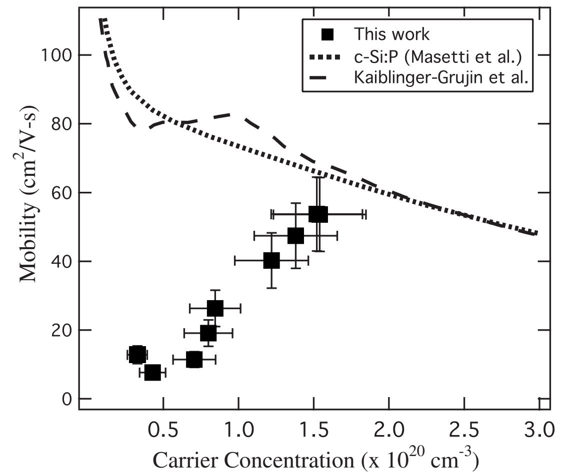

FIG. 5. Mobility as a function of cc for films annealed at 600 °C. The dotted line is fitted to data from c-Si:P samples from Masetti*et al.*

increases, μ flattens out and finally decreases with T. This trend in the mobility with temperature suggests that impurity scattering dominates at the lower ccs, whereas phonon scattering begins to have a larger influence at higher ccs.[19] Electrical conductivity as a function of measurement temperature (not shown) was measured by the Van der Pauw method. For all of the films in this study the conductivity followed the mobility trends of Fig. 6 because the carrier density remained essentially constant over our measurement temperature range (100–320 K).

IV. DISCUSSION

To understand the transport data, we return to Fig. 5 and note the increase in mobility with increasing cc. This trend

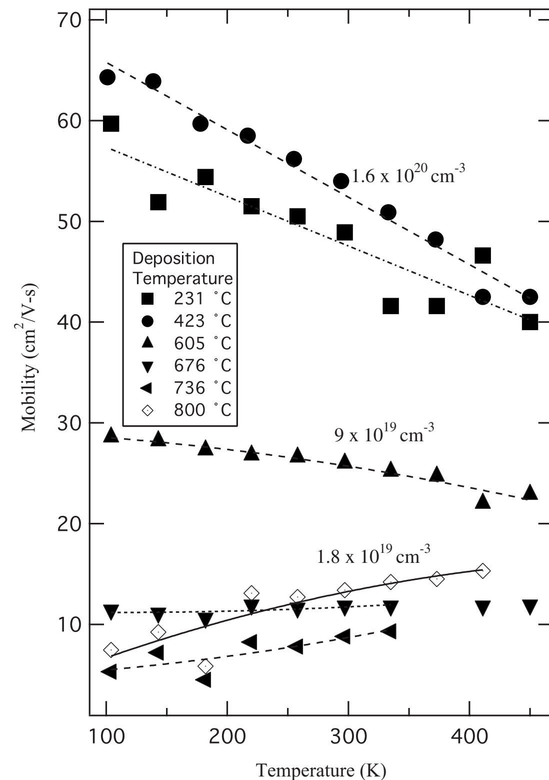

FIG. 6. Mobility as a function of temperature for films of varying ccs.

Downloaded 21 Nov 2011 to 147.8.21.59. Redistribution subject to AIP license or copyright; see http://jap.aip.org/about/rights_and_permissions

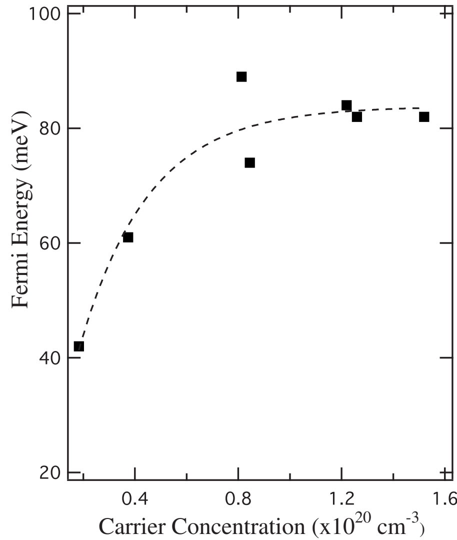

FIG. 7. Fermi energy level, with respect to the bottom of the conduction band, as a function of cc.

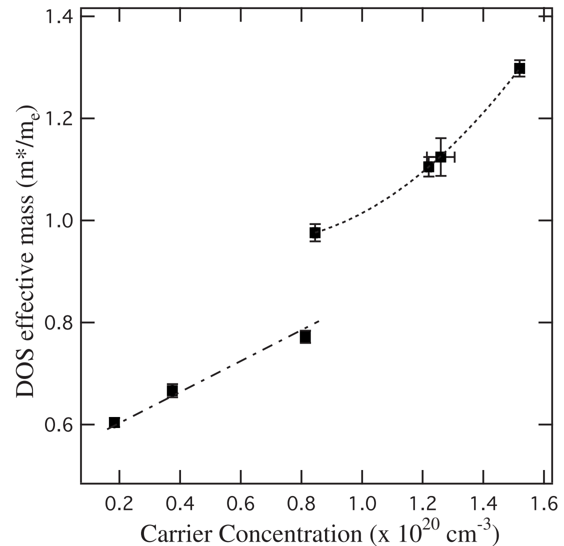

FIG. 8. Measured electron DOS effective mass as a function of cc for P-doped, poly-Si films.

was previously observed in small-grained polycrystalline n- and p-type silicon samples,[20–22] in contrast to the mobility decrease with n seen in c-Si:P.[18] The rapid increase in conductivity with increasing doping concentration in poly-Si films makes them ideal for transparent contacts on semiconducting devices. However, the physical reason for this conductivity increase in heavily doped poly-Si samples is still an open debate. Several authors have argued that grain-boundary barriers[21,22] decrease in scattering efficiency as the doping level increases. Our data do not contradict this hypothesis; however, we believe the main reason for the mobility trend seen in Fig. 5 is a fundamental change in conduction mechanism from an impurity band to the conduction band as cc increases.

Figure 7 shows, as a function of n, the energy difference between the conduction band and the Fermi energy, as calculated with the MFC method.[11] This energy difference ranges from 40 to 80 meV. When we apply Seto's grain-boundary theory[22] to the data of Fig. 6 to calculate grain-boundary energy barriers which must be surmounted (or tunneled through) for grain-to-grain transport; we obtain values of 10–25 meV for all the films. Thus, both room-temperature k_BT and the Fermi energy with respect to the conduction-band minimum for all of the films are significantly larger than the grain-boundary barrier energy, and these barriers therefore would not inhibit the mobility much.

The conclusion that grain-boundary barriers are unimportant to transport (at least above T_d=200 °C) is consistent with the data of Figs. 4(c) and 4(d). First, the mean free path [Fig. 4(c)] is less than a few nanometers in all of the films. As most of the film comprises grains larger than 1 μm, this implies that the scattering controlling the measured transport occurs *within* the grains rather than at the boundaries *between* grains. Second, the femtosecond relaxation times between scattering events [Fig. 4(d)] mean intragrain scattering must dominate because, on average, there would be about 170 scattering events for an electron traversing a 1 μm diameter grain. It should be noted that the data of Figs. 4(d) and 7, so key to our grain-boundary conclusion, are only made possible through the measurement of all four transport coefficients (e.g., effective mass—see Fig. 8). Our earlier Scherrer formula analysis, showing uniform grain sizes in all of the films on the order of micrometers, is consistent with our null conclusion for grain-boundary scattering. One would expect XRD peak broadening in films with grains less than 100 nm in diameter. Even if the films did have such small diameter grains, intragrain scattering would still be expected due to the small mean free path in the films [Fig. 4(c)].

The T-dependence of mobility at high ccs (low T_d) seen in Fig. 6 suggests phonon scattering, and together with the results of Fig. 4(a) indicates that intragrain electronic quality improves with lower deposition temperatures. It should be noted that phononlike scattering has also been seen in high mobility, small-grained (~1 μm) TCO materials[23] as well as in some metals. At low T_d (high n), the electron transport in our films is comparable to that of single-crystal wafers, with an electron mobility of 54 cm^2/V s. The mean free path [Fig. 4(c)] and relaxation time [Fig. 4(d)] confirm the intragrain quality improvement trend at low T_d.

Having ruled out grain boundaries as the dominant transport-limiting mechanism in our films, we next explore the curvature of the transport band by calculating the DOS effective mass (m^*) at the Fermi level from the MFC data.[11] Figure 8 shows m^*/m_e as a function of cc, where m_e is the free-electron mass. It should be emphasized that the low mobilities (<100 cm^2/V s) of silicon at these high ccs limit the experimental techniques available to probe the effective mass: cyclotron and de Haas van Alphen resonance techniques are not applicable.[24] MFC is one of the few techniques available for measuring m^* in low mobility samples. The data of Fig. 8 provide the first *measured* m^* values in any form of silicon at such high ccs. Up to this point, only theoretical band calculations have been offered in the literature.[18] In a perfect single crystal, the Fermi level moves higher in the conduction band with increasing carrier density

Downloaded 21 Nov 2011 to 147.8.21.59. Redistribution subject to AIP license or copyright; see http://jap.aip.org/about/rights_and_permissions

and the effective mass is a measure of the curvature of the band dispersion $E(k)$ at the Fermi energy. The data of Fig. 8 show an increasing effective mass with carrier density reflecting the normal flattening of the $E(k)$ curve as E increases above the band minimum. However, the most striking feature of Fig. 8 is the apparent discontinuity in m^* from 0.79 m_e to 0.99 m_e near $n_{crit}=8\times10^{19}$ cm^{-3}, roughly the cc at which the Nernst coefficient changed sign [Fig. 3(a)]. The m^* values above n_{crit} are consistent with *calculated* DOS effective mass values for silicon.[25] However, m^* values below n_{crit} have a shallower slope (dm^*/dn) than those above n_{crit} and magnitudes that are 20%–40% lower than calculated.[18]

As impurity doping increases within a semiconductor, the spacing between impurity atoms decreases, and the overlap of impurity atom wave functions causes development of extended states and broadening into an impurity band. This Mott or metal-insulator transition[1,26] increases the mobility of the carriers within the lattice suddenly as the impurity concentration increases beyond a critical value sufficient to cause "large" overlap of impurity wave functions. All the films in this study have high enough impurity concentrations to have impurity bands ($>10^{19}$ cm^{-3}),[2] so a Mott transition cannot account for the discontinuity in m^*.

The discontinuity in effective mass seen in Fig. 8 is best explained by a change in transport from an impurity band to the normal conduction band. Most likely, the impurity-band center and conduction-band minimum change little with doping density, but the impurity-band width and Fermi level rise with increasing impurity concentration. Thus, the MFC sampling energy moves from the impurity band into the conduction band with increasing carrier density. The discontinuity in m^* seen in Fig. 8 reflects this transition between bands of very different curvatures. However, when the doping level increases, the lowest lying conduction-band states are likely perturbed by the potentials of the impurities and the curvature of the conduction band is altered.[2] The lowest part of the conduction band, most relevant to transport, now becomes a mixture of the pure conduction band and the impurity band. Mixing a Si:P impurity band with the conduction band should occur at a cc of about 2×10^{19} cm^{-3},[2,27] consistent with our measured n_{crit}. Only at very high cc will electrons move into a nearly unperturbed conduction band and the mobility approaches that of c-Si (Fig. 5).

The hypothesis of an interaction between the impurity band and the conduction band above n_{crit} is supported by susceptibility data in the literature. Quirt and Marko[28] measured the susceptibility of highly P-doped c-Si powders and found a sudden shift from impurity-band conduction to metallic conduction at a critical carrier density of 4×10^{19} cm^{-3}. Ue and Maekawa,[6] studying heavily phosphorus-doped silicon crystals, and later, Brendel *et al.*,[4] studying laser-crystallized polycrystalline P-doped c-Si films, observed related effects. All this work showed that the T-dependence of magnetic susceptibility contains both Curie-like (T-dependent) and Pauli-like (T-independent) paramagnetism contributions, but the Pauli T-dependence dominates at the higher ccs. Curie law paramagnetism is associated with localized, noninteracting spins, and Pauli paramagnetism is due to a free-electron gas, or conduction-band electrons.[28] In other words, as the cc increases, carrier transport shifts away from localized states toward conduction-band-like states.

The mobility (T) data of Fig. 6 also support this idea of shifting transport from an impurity band to the conduction band with increasing cc. At low cc the dominant scattering mechanism is by ionized impurities (localized states). At high cc scattering shifts toward phonon scattering—consistent with transport in an unperturbed conduction band.

Within our model, m^* values below n_{crit} reflect transport in an impurity band, while values above the critical density reflect the curvature of the "normal" silicon conduction band. According to Conwell,[2] band theory should apply to both bands at these high ccs and therefore the MFC should be applicable. Our measured m^* values strongly support this claim. The change in m^* with n within each band suggests that neither is exactly parabolic. One might expect the effective mass in the impurity band to be higher than the effective mass in silicon rather than lower because of the relatively small overlap in impurity wave functions compared to silicon. As interatomic distances between isolated P atoms decrease and an impurity band begins to form, the newly formed impurity band would be narrow and therefore have little curvature and nearly infinite effective mass. On the other extreme, as the spacing between P atoms approaches that of crystalline P, the "impurity" band within the silicon lattice might mimic the band structure of crystalline P. In this case, the impurity-band curvature would give the small effective mass values of electrons in P, which is only 34% of the corresponding value in silicon.[25] At our measured n_{crit}, we expect the characteristic spacing between P atoms to be about ten times larger than in crystalline P. Evidently a superposition or mixing of states between silicon's conduction band and a P impurity band gives effective mass values in the range seen in Fig. 8. Continued experimental and theoretical work is needed to understand the nature of conduction in impurity bands in semiconductors and to better understand the transition from impurity band to conduction-band transport we have observed. Our experimental values of m^* for both an impurity band and the conduction band for silicon and experimental determination of n_{crit} should offer valuable guidance for future studies. It will be important to measure the effective mass of c-Si samples over the same cc range. This might reveal the root cause of the poorer transport in poly-Si compared with crystalline Si.

V. SUMMARY

We grew phosphorus-doped a-Si:H films by the HWCD technique and annealed them to form polycrystalline silicon thin films on glass substrates. Varying the deposition temperature from 150 to 820 °C reveals an increase in electron transport with increasing cc, primarily due to an improvement in electron mobility (up to 82% of crystalline Si). Measured structural and transport data by the MFC of our poly-Si films suggest that the improved transport can be qualitatively accounted for by a change in scattering mechanism from ionized impurity to phonon scattering over this cc range. Our experimental measurements of effective mass values show

Downloaded 21 Nov 2011 to 147.8.21.59. Redistribution subject to AIP license or copyright; see http://jap.aip.org/about/rights_and_permissions

directly that as the cc increases, there is a shift from impurity band to conduction-band transport. The previous results on T-dependent magnetic susceptibility in heavily doped poly-Si confirm our result. Our data establish the existence of an effective mass for impurity bands and experimentally determines the critical cc for impurity band and conduction-band overlap in silicon.

ACKNOWLEDGMENTS

The authors thank Dr. Paul Stradins of NREL for assistance with optical measurement of crystallization and for several helpful suggestions. Dr. Klaus Lips of Helmholtz Centre Berlin is gratefully acknowledged for helpful discussions about magnetic susceptibility. This work was supported by the U.S. DOE under Contract No. DE-AC36-99GO10337.

[1]N. F. Mott, Can. J. Phys. **34**, 1356 (1956).
[2]E. M. Conwell, Phys. Rev. **103**, 51 (1956).
[3]M. Imada, A. Fujimori, and Y. Tokura, Rev. Mod. Phys. **70**, 1039 (1998).
[4]K. Brendel, N. H. Nickel, K. Lips, and W. Fuhs, J. Non-Cryst. Solids **338–340**, 262 (2004).
[5]J. D. Quirt and J. R. Marko, Phys. Rev. Lett. **26**, 318 (1971).
[6]H. Ue and S. Maekawa, Phys. Rev. B **3**, 4232 (1971).
[7]J.-H. Park, I.-H. Song, and M.-K. Han, Thin Solid Films **515**, 7402 (2007).
[8]T. Matsuyama, N. Terada, T. Baba, T. Sawada, S. Tsuge, K. Wakisaka, and S. Tsuda, J. Non-Cryst. Solids **198–200**, 940 (1996).
[9]P. Widenborg and A. G. Aberle, Adv. OptoElectron. **2007**, 24584 (2007).
[10]M. A. Green, P. A. Basore, N. Chang, D. Clugston, R. Egan, R. Evans, D. Hogg, S. Jarnason, M. Keevers, P. Lasswell, J. O'Sullivan, U. Schubert, A. Turner, S. R. Wenham, and T. Young, Sol. Energy **77**, 857 (2004).
[11]D. L. Young, T. J. Coutts, and V. I. Kaydanov, Rev. Sci. Instrum. **71**, 462 (2000).
[12]P. Stradins, D. L. Young, Y. Yan, E. Iwaniczko, Y. Xu, R. Reedy, H. M. Branz, and Q. Wang, Appl. Phys. Lett. **89**, 121921 (2006).
[13]D. L. Young, D. L. Williamson, P. Stradins, Y. Xu, L. Gedvilas, A. H. Mahan, H. Branz, and Q. Wang, Appl. Phys. Lett. **89**, 161910 (2006).
[14]B. D. Cullity, *Elements of X-Ray Diffraction* (Addison-Wesley, Reading, MA, 1978).
[15]D. L. Young, T. J. Coutts, V. I. Kaydanov, A. S. Gilmore, and W. P. Mulligan, J. Vac. Sci. Technol. A **18**, 2978 (2000).
[16]D. Song, P. Widenborg, A. Straub, P. Campbell, N. Chaungsuwanich, Y. Huang, and A. G. Aberle, *31st IEEE Photovoltaic Specialists Conference* (IEEE Electron Devices Society, Lake buena Vista, FL, 2005), p. 1217.
[17]B. M. Askerov, *Electron Transport Phenomena in Semiconductors* (World Scientific, Singapore, 1994).
[18]G. Masetti, M. Severi, and S. Solmi, IEEE Trans. Electron Devices **30**, 764 (1983).
[19]S. S. Li, *Semiconductor Physical Electronics* (Plenum, New York, 1993).
[20]M. E. Cowher and T. O. Sedgwick, J. Electrochem. Soc. **119**, 1565 (1972).
[21]K. V. Maydell, S. Brehme, N. H. Nickel, and W. Fuhs, Thin Solid Films **487**, 93 (2005).
[22]J. Y. W. Seto, J. Appl. Phys. **46**, 5247 (1975).
[23]Y. Yoshida, D. M. Wood, T. A. Gessert, and T. J. Coutts, Appl. Phys. Lett. **84**, 2097 (2004).
[24]Due to the constraint that the product $\mu B \gg 1$ $(\omega\tau \gg 1)$ so that electrons complete at least one orbit before they are scattered. For typical laboratory magnetic fields, mobilities about 10^5 cm^2/V s are needed.
[25]L. I. Berger, *Semiconductor Materials* (CRC, New York, 1997).
[26]N. F. Mott, Philos. Mag. **6**, 287 (1961).
[27]W. Baltensperger, Philos. Mag. **44**, 1355 (1953).
[28]J. D. Quirt and J. R. Marko, Phys. Rev. B **5**, 1716 (1972).
[29]M. Birkholz, *Thin Film Analysis by X-Ray Scattering* (Wiley-VCH, Weinheim, 2006).

Downloaded 21 Nov 2011 to 147.8.21.59. Redistribution subject to AIP license or copyright; see http://jap.aip.org/about/rights_and_permissions